

# Cold sintering process for fabrication of a high volumetric capacity $\text{Li}_4\text{Ti}_5\text{O}_{12}$ anode

Joo-Hwan Seo<sup>a</sup>, Kris Verlinde<sup>a</sup>, Ramakrishnan Rajagopalan<sup>b,c</sup>, Enrique D. Gomez<sup>a,c,d</sup>, Thomas E. Mallouk<sup>e</sup>, Clive A. Randall<sup>a,c,\*</sup>

<sup>a</sup> Department of Materials Science and Engineering, The Pennsylvania State University, University Park, PA 16802, USA

<sup>b</sup> Department of Engineering, The Pennsylvania State University, Dubois, PA 15801, USA

<sup>c</sup> Materials Research Institute, The Pennsylvania State University, University Park, PA 16802, USA

<sup>d</sup> Department of Chemical Engineering, The Pennsylvania State University, University Park, PA 16802, USA

<sup>e</sup> Department of Chemistry, The Pennsylvania State University, University Park, PA, 16802, USA

## ARTICLE INFO

### Keywords:

Cold sintering process  
Lithium titanate  
Composite electrode  
Volumetric capacity

## ABSTRACT

The cold sintering process (CSP) is useful for densifying lithium ion battery composite electrodes to achieve higher volumetric capacity density. Lithium titanate is one of the most promising anode materials to replace graphite in conventional anodes, as it enhances safety in large scale applications. A densified binder-free LTO based anode was fabricated by the cold sintering process. The composite anode was first formed by tape casting with a binder and then was heat treated to remove the binder. The binder-free composite was humidified with water to provide a transient liquid phase and then moved onto a current collector. The wetted composite was cold sintered at 120 °C under a uniaxial pressure of 500 MPa and directly deposited on a current collector. The density of the LTO/CNF composite anode was 2.82 g/cm<sup>3</sup> (87% relative density). The volumetric capacity densities of the cold sintered anodes were found to be ~380 mAh/cm<sup>3</sup>.

## 1. Introduction

Lithium ion batteries (LiBs) are attractive for large scale electric energy storage applications such as electric vehicles and grid storage with renewable energy power generation due to their high energy density, long cycle life and relative low cost [1–6]. One of the key issues for LiBs in large scale energy storage applications is safety, as the operating environments and total stored energy are more extreme than those found in portable electronic devices [7–9]. Conventional LiBs employing a graphite-based anode have safety issues due to the possibility of internal short circuiting originating from lithium dendrite growth [10–14]. Lithium titanate ( $\text{Li}_4\text{Ti}_5\text{O}_{12}$ , LTO) with a cubic spinel ( $\text{AB}_2\text{O}_4$ , A = Li, B = Li, Ti) structure is one of the most promising alternative anode materials for Li-ion batteries because of advantages in enhanced safety, high operating voltage, and relatively high capacity (175 mAh/g). Moreover, LTO is easy to fabricate and has good cycling performance [9,15–20].

Despite these advantages of LTO, the low volumetric capacity of LTO-based electrodes is a challenge for its use in mainstream applications [1,9]. In order for LTO to be useful in portable electronic devices, for EVs, smart grids, and even smaller multilayer ceramic batteries the

volumetric capacity must be increased [21–23]. LTO (175 mAh/g, 613 mAh/cm<sup>3</sup>) has a lower theoretical gravimetric and volumetric capacity than graphite (372 mAh/g, 837 mAh/cm<sup>3</sup>), the anode material that is typically used in commercial LiBs [13,24]. The theoretical density of LTO (3.5 g/cm<sup>3</sup>) is much lower than most oxides. For example, most oxide-type cathode materials have a density of ~5 g/cm<sup>3</sup>. On a practical level, this means that we must increase the packing density of the LTO-based anode in order to increase the overall volumetric energy density of Li-ion cells with conventional cathodes. Some of the present research strategies are focused on developing fabrication processes for LTO-based materials with high tap density to improve their volumetric performance. This involves powder synthesis and powder packing strategies with size distributions such as hydrothermal methods, the sol–gel route, spray drying, and carbon coating of the powders to minimize the inactive binder content [3,8,25–28]. With cold sintering there is no need to use binders in the final assembly or to use spray dried particles, thereby eliminating several processing steps. Typically, inactive materials can take up to 50% of the total volume of composite electrodes fabricated by conventional tape-casting and/or calendaring processes [29,30]. These inactive components include materials such as conductive carbon, binders and pores [31]. Therefore,

\* Corresponding author at: Department of Materials Science and Engineering, The Pennsylvania State University, University Park, PA 16802, USA.  
E-mail address: [car4@psu.edu](mailto:car4@psu.edu) (C.A. Randall).

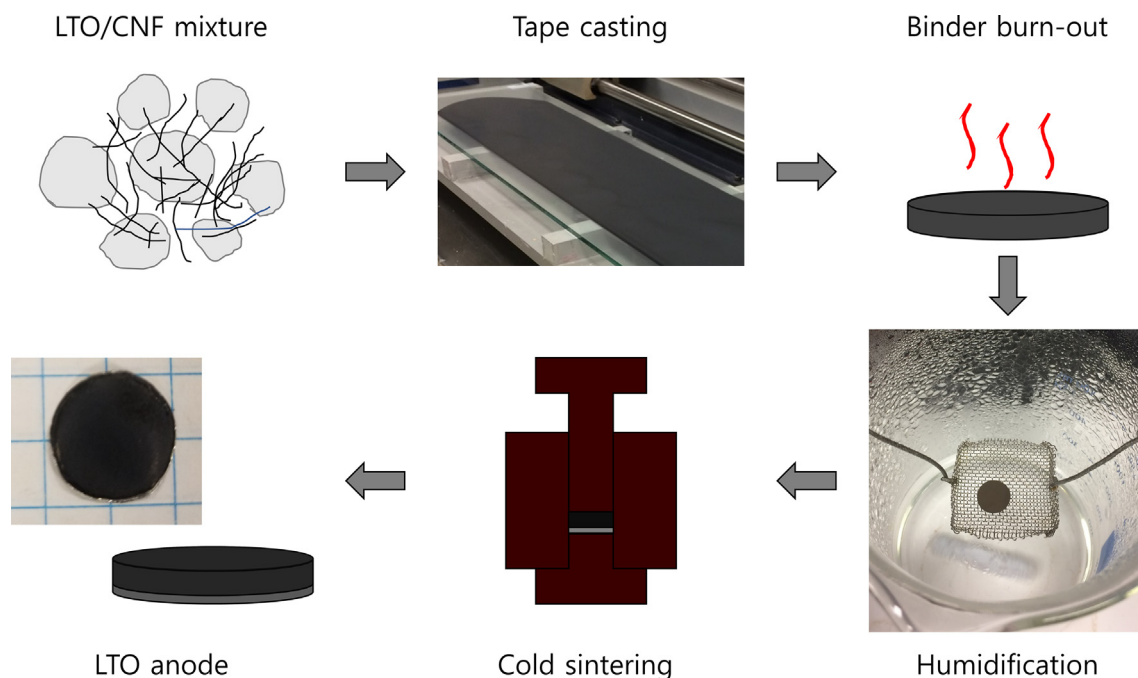


Fig. 1. A schematic illustration of the fabrication procedure for the LTO/CNF anode using the cold sintering process.

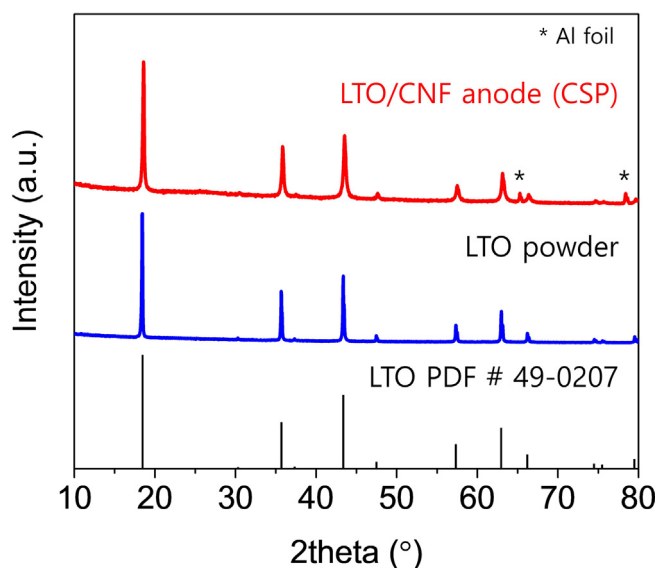


Fig. 2. X-ray diffraction patterns of LTO powder and the cold sintered LTO/CNF composite, along with a LTO reference pattern. Peaks from the aluminum substrate are marked with asterisks.

a process that enables the removal of binders and reduces the porosity is needed to increase the volumetric energy density of LTO electrodes.

Recently a low temperature sintering process, named cold sintering process, was developed for the densification of various families of ceramics and ceramic-based composites [32]. The cold sintering process utilizes a transient aqueous liquid phase that assists the dissolution and precipitation processes, enabling densification of particulate materials under uniaxial pressure at a relatively low sintering temperature ( $< 300\text{ }^{\circ}\text{C}$ ). The cold sintering process can achieve relative densities up to 90% and beyond [33,34]. A wide range of ceramics and ceramic-based composites with a various functional materials, including semiconductors, ferroelectrics, thermoelectrics, two-dimensional and structural materials, have all been densified successfully by cold sintering [33,35–40]. This low temperature densification process is useful for

densification of battery materials such as composite electrodes, solid electrolytes and even for fabrication of all-solid-state batteries. There have been several studies reporting the application of the cold sintering process for the densification of the battery materials, for example cathodic olivine structured  $\text{LiFePO}_4$ , solid electrolytes such as NASICON (sodium (Na) superionic conductor,  $\text{NaM}_2(\text{PO}_4)_3$  ( $M = \text{Ge, Ti, Zr}$ ))-type  $\text{Li}_{1.5}\text{Al}_{0.5}\text{Ge}_{1.5}(\text{PO}_4)_3$ , to increase the density and volumetric capacity of the electrodes as well as the ionic conductivity of solid electrolytes [41–46].

The objective of this study was to explore cold sintering to improve the volumetric capacity density of an anode material, specifically LTO-based materials. The structure-property-processing relations have been accessed with this system and are discussed in the context of electrochemical performance.

## 2. Experimental approach

A green tape LTO anode was fabricated by the tape-casting method previously reported by our group for cathodes [47,48]. LTO ceramic powders purchased from MTI Corporation were used as the active material. Carbon nanofiber (CNF) was provided by Mitsubishi Materials, Inc. and used to increase the electronic conductivity. A mixture of LTO and CNF (90/10 w/w) was added to a polypropylene container with milling media based on yttria-stabilized  $\text{ZrO}_2$  beads and an ethanol solvent, where they were ball milled for over 24 h. After drying the slurry, the powder mixture was then ground with a mortar and pestle. A slurry was prepared by mixing these powders, binder (QPAC40, Empower Materials) and plasticizer (S-160, Tape Casting Warehouse). The mass ratio of the LTO/CNF powder mixture, binder, plasticizer, and solvent in the slurry was 17.8:7.3:0.3:74.2. After stirring overnight, a  $70\text{ }\mu\text{m}$ -thick green tape was cast with a doctor blade onto a mylar support film. The green tape was then dried at room temperature overnight and punched into disks with a diameter of 12 mm. The samples were heat treated at  $250\text{ }^{\circ}\text{C}$  for 1 h at a ramp rate of  $3\text{ }^{\circ}\text{C}/\text{min}$  in order to burn out all the organics. The binder-free anode composite tape was then composed of 90 wt% LTO and 10 wt% CNF. The LTO/CNF composite film was then humidified for 30 min over water heated at  $80\text{ }^{\circ}\text{C}$  on a hot plate. This step enables the uptake of the transient liquid phase through the vapor, and thereby avoids problematic capillary

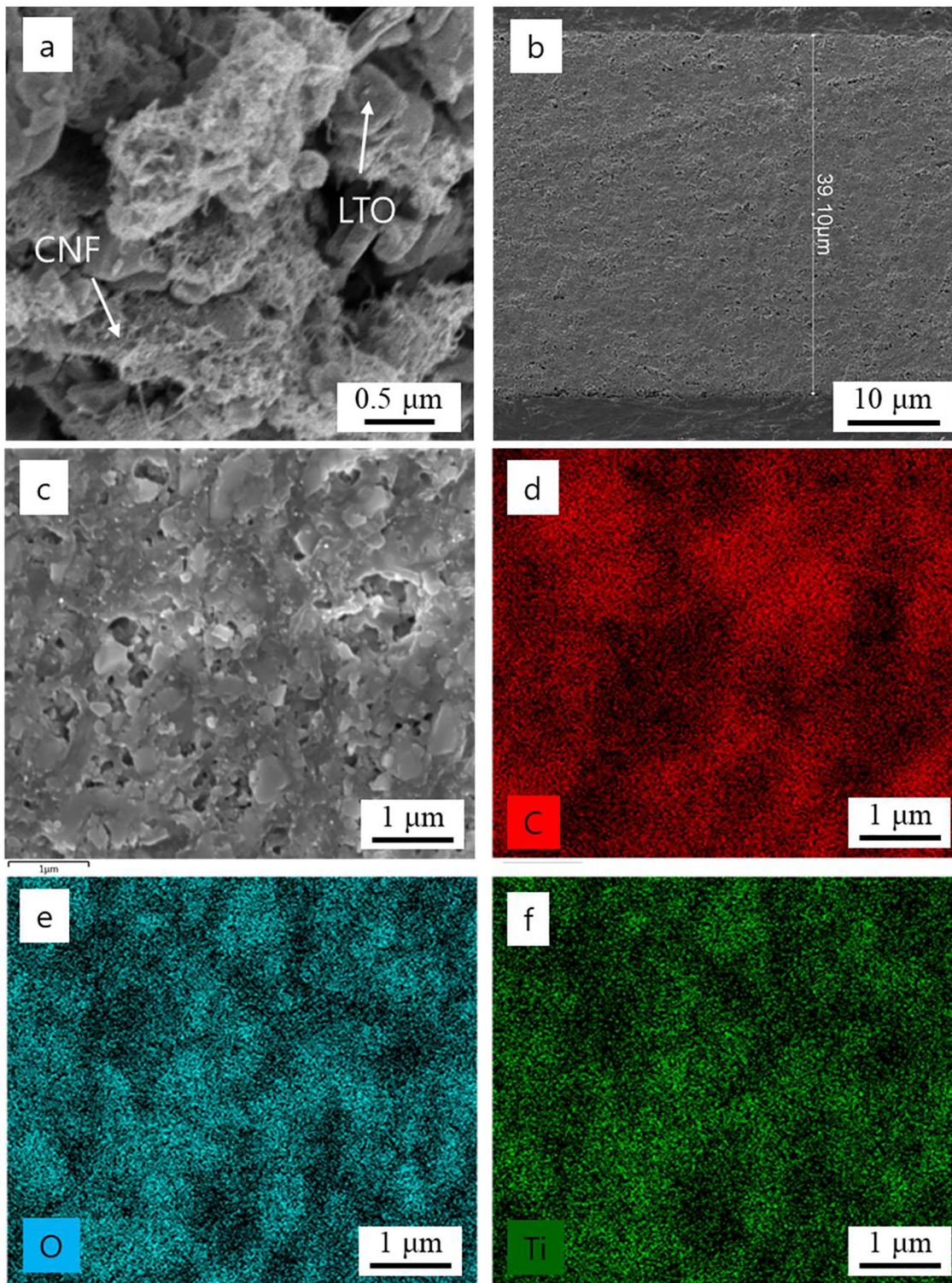


**Fig. 3.** SEM images of (a) ball milled powder mixture of LTO and CNF, (b–f) cross-sectional surface of a cold sintered anode at different magnifications with EDS maps.

forces induced by adding the transient phase directly as a liquid. The wetted tape was transferred onto aluminum foil, which was used both as a substrate and a current collector. The cold sintered process was done using a laboratory platen hot press at 120 °C for 30 min under 500 MPa.

The density of the cold sintered electrode was determined by a geometric method using the weight/volume ratio of the electrodes. The volume of the electrode was calculated by multiplying the area and

thickness of the electrodes. The relative density was computed based on the mass fraction and intrinsic densities of 3.5 and 1.95 g/cm<sup>3</sup> for the LTO and CNF phases, respectively. The crystalline phases present in the cold sintered tape were determined by X-ray diffraction using a PANalytical Empyrean diffractometer with a Cu-Kα radiation source at a scan rate of 0.026° between 10 and 80 degrees 2-theta. The microstructural and elemental distributions of the cold sintered anode were characterized using scanning electron microscopy (SEM), NanoSEM

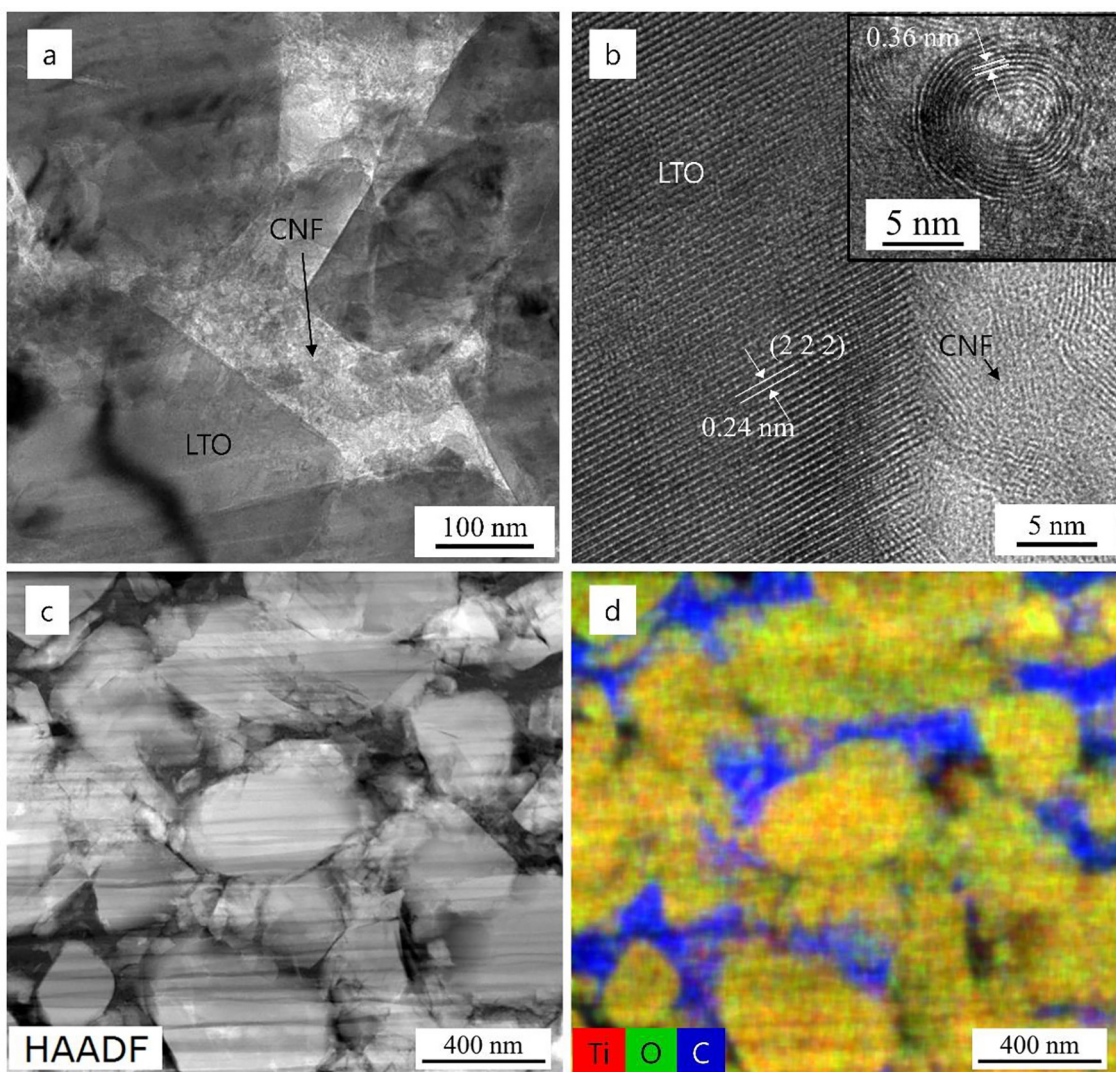


**Fig. 4.** TEM and EDS mapping images of a cold sintered LTO/CNF composite anode, (a) and (c) show the dense microstructure, and (b) has an inset with a graphitic turbostratic structure within the carbon fibers.

630 and transmission electron microscopy (TEM), using a FEI Talos with energy dispersive spectroscopy (EDS) to assess grain structure and carbon distribution. Fractured cross-sectional SEM characterization was performed by using a polished electrode. The TEM specimen was prepared by a standard sample preparation process to obtain electron transparency including polishing and ion beam milling (Gatan, PIPS II).

The electrochemical performance was evaluated with a 2032 type coin cell assembled in a MBraun argon-filled glove box with a cold sintered LTO electrode as the working electrode. Lithium foil was used as the reference and counter electrode. A liquid electrolyte, 1 M lithium hexafluorophosphate solution in ethylene carbonate and dimethyl carbonate (1 M LiPF<sub>6</sub> with EC/DME (1:1 v/v), Sigma-Aldrich), was used with a porous polyvinylidene difluoride membrane (Amersham) as a separator. The electrochemical measurements were conducted with a galvanostatic charge/discharge system (Neware BTS4000) in the range of 1–2.5 V at charge/discharge rates of 0.1–1C at room temperature. Cyclic voltammetry was also performed in the range of 0.8–2.6 V vs Li<sup>+</sup>/Li at a scan rate of 0.1 mV/s. The specific capacity of the anodes was calculated based on the mass of active material. The volumetric capacity was computed using the total volume of the anode not including the aluminum current collector.

### 3. Results and discussion

**Fig. 1** illustrates the basic fabrication process of binder-free LTO/CNF composite anodes using the cold sintering process.

A phase analysis was conducted to confirm the phase purity of the LTO composite after the cold sintering process. X-ray diffraction patterns of pure LTO powder, the cold sintered LTO electrode and a reference pattern of LTO are shown in **Fig. 2**. All the peaks could be assigned to the LTO phase, and the relative intensities were similar suggesting there was no preferred orientation in the sintered sample. The only other peaks identified were those from the Al foil substrates.

**Fig. 3** shows images of a powder mixture of LTO/CNF and cross-sectional images of a cold sintered LTO/CNF composite anode. As shown in **Fig. 3a**, it can be observed that the LTO and CNF powders were homogeneously dispersed through the wet ball milling process. A low magnification image in cross-section of the cold sintered composite anode is shown in **Fig. 3b**. The cold sintered LTO anodes were ~35 μm-thick and the mass loading of active materials was ~9 mg/cm<sup>2</sup>. The average density of the cold sintered electrodes was 2.82 g/cm<sup>3</sup> corresponding to 87.0% of the theoretical density for the composite. As shown in **Fig. 3c**, we see a highly densified composite anode with low porosity, which is advantageous for maximizing the volumetric capacity of the cold sintered anode. As EDS mapping images show in

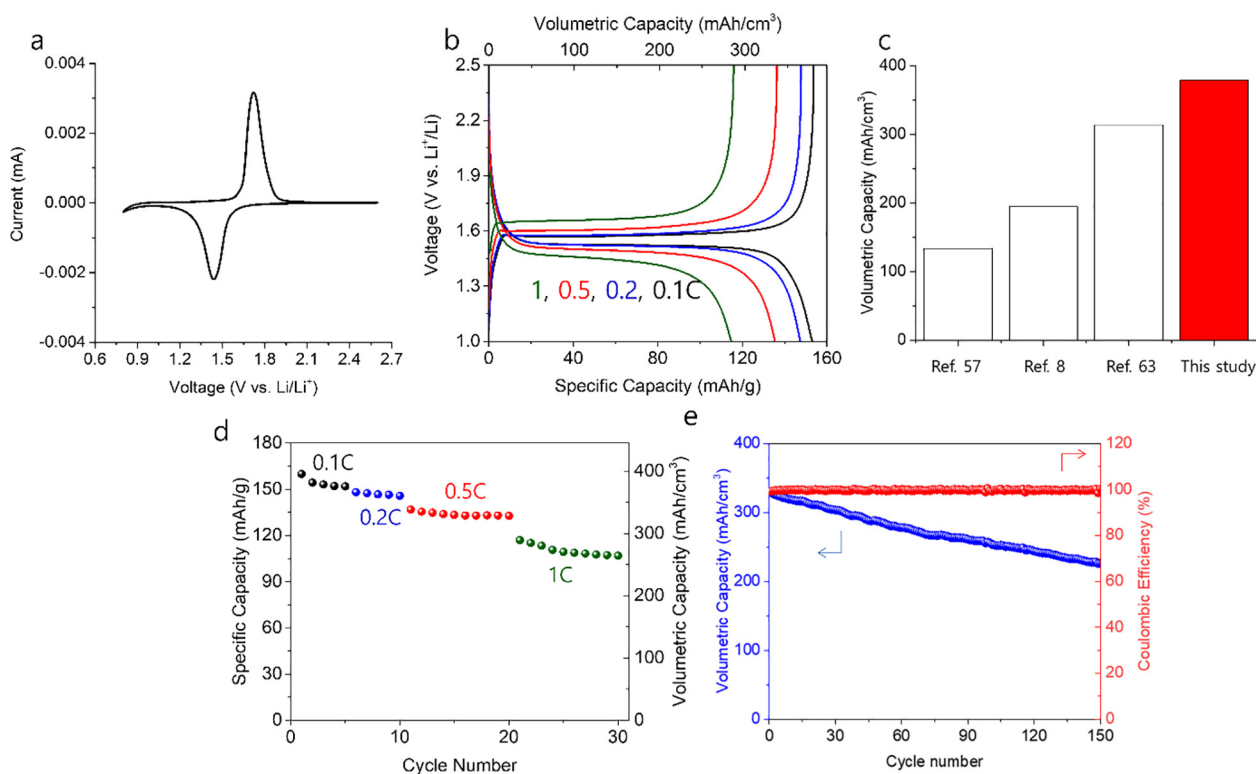


**Fig. 5.** Electrochemical performance of a cold sintered LTO/CNF anode: (a) CV curve at a scan rate of 0.1 mV/s, (b) voltage profiles and capacities, (c) Comparison of the volumetric capacity of the cold sintered LTO anode to those previously reported at 0.1C, (d) Rate capabilities at different C-rates: 0.1, 0.2, 0.5, and 1C, and (e) cycling performance at 0.2C.

Fig. 3d–f, the LTO and CNF were uniformly distributed between the LTO grains, and throughout the thick films. The carbon nanofiber network between active materials in the highly densified electrode structure is distributed to provide a continuous pathway, with their high conductivity and high aspect ratio. Therefore, the nanofiber network interconnects the current collector and the electroactive LTO phase, thus enabling exchange of the Li-ion [49].

A more detailed analysis of the microstructure of the cold sintered composite was performed using TEM. Fig. 4 shows LTO grains and the carbon phase distributed in the cold sintered composite. Dense microstructures in the entire region were observed, with very little porosity between the LTO phase and the carbon. The inset image in 4b shows some of the details of the carbon, where fringes can be observed corresponding to the graphitic layers in the carbon fibers. The inset shows the presence of carbon onions at the interface. This result is quite unprecedented as the transformation of allotropes with tubular morphology such as carbon nanotubes and nanofibers to spherical carbon onions usually requires a localized pressure as high as 10 GPa and temperatures greater than 2000 °C [50–52]. Such transformations have been shown to be initiated in carbon nanotubes through laser irradiation, spark plasma sintering, hydrogen plasma post treated and direct high temperature high pressure treatment [53–56]. In this study, we show that a similar transformation can occur under cold sintering conditions through rupture of carbon nanofibers to yield bent graphitic sheets which can then be transformed into onion-like rings characterized by layer spacings of  $\sim 0.36$  nm.

CV measurement was performed to investigate the phase transformation associated with the lithium insertion/extraction in the LTO lattice. Well-defined reversible redox peaks at 1.72/1.44 V are observed as expected, corresponding to the redox reaction of  $\text{Ti}^{4+}/\text{Ti}^{3+}$  [57–59]. The electrochemical performance of the cold sintered LTO/CNF composite anodes were evaluated by galvanostatic measurements in the voltage range of 1–2.5 V to fully utilize the capacity of the LTO. Charge/discharge rates between 0.1C and 1C were applied to evaluate the rate

capabilities of the cold sintered anodes. The voltage profiles of first cycle of each C-rate measurement are shown in Fig. 5b. The cold sintered LTO/CNF composite anode exhibits flat plateaus around 1.55 V during charge/discharge, as typically observed in other reported LTO-based anodes [60–62]. The discharge voltage dropped with increasing current density due to polarization. As expected, the capacity decreased at higher current density. At the low rate of 1C, the cold sintered LTO anode delivered a specific capacity and volumetric capacity of 153 mAh/g and 379 mAh/cm<sup>3</sup>, respectively. It should be noted that the volumetric capacity of cold sintered anodes is much higher than those of LTO-based electrodes, measured at the same current density of 0.1C, previously reported in the literature as shown in Fig. 5b [8,57,63]. The high volumetric capacity is attributed to the highly densified and binder-free structure of the cold sintered electrodes, which minimizes the volume of inactive components. At a high C-rate of 1C, the cold sintered LTO composite electrode exhibits a gravimetric and volumetric capacity of 115 mAh/g and 285 mAh/cm<sup>3</sup>, respectively. It may be possible to further improve the rate capability of the cold sintered LTO/CNF electrodes by introducing a conductive carbon layer on the LTO or by carbon coating to enhance electronic conductivity, and by employing finer or nano-sized primary LTO particles to reduce the lithium-ion diffusion distance.

When the cycling performance of the cold sintered composite electrode was evaluated at 0.2C over 150 cycles, the capacity faded to 69% of its initial value. However, the cold sintered composite electrode still exhibited a volumetric capacity of 225 mAh/cm<sup>3</sup> after 150 cycles. The coulombic efficiency was  $\sim 99.8\%$  over all measurements taken.

#### 4. Conclusions and summary

In conclusion, high volumetric capacity anodes based on LTO for enhanced safety Li-ion batteries can be fabricated by the cold sintering process. A binder-free tape of LTO/CNF composite was prepared by tape-casting followed by binder burn-out. The thin composite anode

was densified at 120 °C by cold sintering. The density of the cold sintered electrodes was 87% of the theoretical density and a highly densified microstructure was observed. The cold sintered composite anode delivered a high volumetric capacity of ~380 mAh/cm<sup>3</sup> at low current density and showed good cycling stability with a volumetric capacity of 225 mAh/g after 150 cycles at 0.2C. These results indicated that the cold sintering process is an effective method for improving the volumetric capacity of electrodes for Li-ion batteries. These results suggest that it may be possible to use the cold sintering process to fabricate high density composite electrolytes and all-solid-state batteries as well.

### Declaration of Competing Interest

The authors declare that they have no known competing financial interests or personal relationships that could have appeared to influence the work reported in this paper.

### Acknowledgements

This work was supported by the Advanced Research Projects Agency within the U.S. Department of Energy under grant No. DE-AR0000766. The authors would like to thank the MRI-MCL at The Pennsylvania State University for the use of characterization facilities.

### References

- [1] K. Amine, I. Belharouak, Z. Chen, T. Tran, H. Yumoto, N. Ota, S.T. Myung, Y.K. Sun, Nanostructured anode material for high-power battery system in electric vehicles, *Adv. Mater.* 22 (2010) 3052–3057, <https://doi.org/10.1002/adma.201000441>.
- [2] B. Zhao, R. Ran, M. Liu, Z. Shao, A comprehensive review of Li<sub>4</sub>Ti<sub>5</sub>O<sub>12</sub>-based electrodes for lithium-ion batteries: the latest advancements and future perspectives, *Mater. Sci. Eng. R Rep.* 98 (2015) 1–71, <https://doi.org/10.1016/j.mser.2015.10.001>.
- [3] H.-G. Jung, M.W. Jang, J. Hassoun, Y.-K. Sun, B. Scrosati, A high-rate long-life Li<sub>4</sub>Ti<sub>5</sub>O<sub>12</sub>/Li[Ni<sub>0.45</sub>Co<sub>0.1</sub>Mn<sub>1.45</sub>]O<sub>4</sub> lithium-ion battery, *Nat. Commun.* 516 (2011), <https://doi.org/10.1038/ncomms1527>.
- [4] A. Mauger, C.M. Julien, A. Paoletta, M. Armand, K. Zaghib, A comprehensive review of lithium salts and beyond for rechargeable batteries: progress and perspectives, *Mater. Sci. Eng. R Rep.* 134 (2018) 1–21, <https://doi.org/10.1016/j.mser.2018.07.001>.
- [5] A. Tornheim, J.C. Garcia, R. Sahore, H. Iddir, I. Bloom, Z. Zhang, Decomposition of phosphorus-containing additives at a charged NMC surface through potentiostatic holds, *J. Electrochem. Soc.* 166 (2019) A440–A447, <https://doi.org/10.1149/2.0951902jes>.
- [6] Z. Yao, X. Xia, Y. Zhang, D. Xie, C. Ai, S. Lin, Y. Wang, S. Deng, S. Shen, X. Wang, Y. Yu, J. Tu, Superior high-rate lithium-ion storage on Ti<sub>2</sub>Nb<sub>10</sub>O<sub>29</sub> arrays via synergistic TiC/C skeleton and N-doped carbon shell, *Nano Energy.* 54 (2018) 304–312, <https://doi.org/10.1016/j.nanoen.2018.10.024>.
- [7] X. Sun, P.V. Radovanovic, B. Cui, Advances in spinel Li<sub>4</sub>Ti<sub>5</sub>O<sub>12</sub> anode materials for lithium-ion batteries, *New J. Chem.* 39 (2015) 38–63, <https://doi.org/10.1039/c4nj01390e>.
- [8] H.G. Jung, J. Kim, B. Scrosati, Y.K. Sun, Micron-sized, carbon-coated Li<sub>4</sub>Ti<sub>5</sub>O<sub>12</sub> as high power anode material for advanced lithium batteries, *J. Power Sour.* 196 (2011) 7763–7766, <https://doi.org/10.1016/j.jpowsour.2011.04.019>.
- [9] Z. Chen, I. Belharouak, Y.K. Sun, K. Amine, Titanium-based anode materials for safe lithium-ion batteries, *Adv. Funct. Mater.* 23 (2013) 959–969, <https://doi.org/10.1002/adfm.201200698>.
- [10] S.S. Zhang, The effect of the charging protocol on the cycle life of a Li-ion battery, *J. Power Sour.* 161 (2006) 1385–1391, <https://doi.org/10.1016/j.jpowsour.2006.06.040>.
- [11] T.-F. Yi, L.-J. Jiang, J. Shu, C.-B. Yue, R.-S. Zhu, H.-B. Qiao, Recent development and application of Li<sub>4</sub>Ti<sub>5</sub>O<sub>12</sub> as anode material of lithium ion battery, *J. Phys. Chem. Solids* 71 (2010) 1236–1242, <https://doi.org/10.1016/j.jpcs.2010.05.001>.
- [12] C. Wang, S. Wang, Y.B. He, L. Tang, C. Han, C. Yang, M. Wagemaker, B. Li, Q.H. Yang, J.K. Kim, F. Kang, Combining fast Li-ion battery cycling with large volumetric energy density: grain boundary induced high electronic and ionic conductivity in Li<sub>4</sub>Ti<sub>5</sub>O<sub>12</sub> spheres of densely packed nanocrystallites, *Chem. Mater.* 27 (2015) 5647–5656, <https://doi.org/10.1021/acs.chemmater.5b02027>.
- [13] W.J. Zhang, A review of the electrochemical performance of alloy anodes for lithium-ion batteries, *J. Power Sour.* 196 (2011) 13–24, <https://doi.org/10.1016/j.jpowsour.2010.07.020>.
- [14] A. Tornheim, S. Sharifi-Asl, J.C. Garcia, J. Bareño, H. Iddir, R. Shahbazian-Yassar, Z. Zhang, Effect of electrolyte composition on rock salt surface degradation in NMC cathodes during high-voltage potentiostatic holds, *Nano Energy* 55 (2019) 216–225, <https://doi.org/10.1016/j.nanoen.2018.10.065>.
- [15] E. Environ, Carbon-coated nano-sized Li<sub>4</sub>Ti<sub>5</sub>O<sub>12</sub> nanoporous micro-sphere as anode material for high-rate lithium-ion batteries, (2011) pp. 4016–4022. doi:10.1039/c1ee01680f.
- [16] T. Yuan, Z. Tan, C. Ma, J. Yang, Z.-F. Ma, S. Zheng, Challenges of spinel Li<sub>4</sub>Ti<sub>5</sub>O<sub>12</sub> for lithium-ion battery industrial applications, *Adv. Energy Mater.* 7 (2017) 1601625, <https://doi.org/10.1002/aenm.201601625>.
- [17] C. Chen, R. Agrawal, C. Wang, High performance Li<sub>4</sub>Ti<sub>5</sub>O<sub>12</sub>/Si composite anodes for li-ion batteries, *Nanomaterials* 1469–1480 (2015), <https://doi.org/10.3390/nano5031469>.
- [18] K. Nakahara, R. Nakajima, T. Matsushima, H. Majima, Preparation of particulate Li<sub>4</sub>Ti<sub>5</sub>O<sub>12</sub> having excellent characteristics as an electrode active material for power storage cells, *J. Power Sour.* 117 (2003) 131–136, [https://doi.org/10.1016/S0378-7753\(03\)00169-1](https://doi.org/10.1016/S0378-7753(03)00169-1).
- [19] Z. Yao, X. Xia, D. Xie, Y. Wang, C. ao Zhou, S. Liu, S. Deng, X. Wang, J. Tu, Enhancing ultrafast lithium ion storage of Li<sub>4</sub>Ti<sub>5</sub>O<sub>12</sub> by tailored TiC/C core/shell skeleton plus nitrogen doping, *Adv. Funct. Mater.* 28 (2018) 1–8, <https://doi.org/10.1002/adfm.201802756>.
- [20] C.A. Zhou, X. Xia, Y. Wang, Z. Yao, J. Wu, X. Wang, J. Tu, Pine-needle-like Cu–Co skeleton composited with Li<sub>4</sub>Ti<sub>5</sub>O<sub>12</sub> forming core-branch arrays for high-rate lithium ion storage, *Small* 14 (2018) 1–9, <https://doi.org/10.1002/smll.201704339>.
- [21] N. Nitta, G. Yushin, High-capacity anode materials for lithium-ion batteries: choice of elements and structures for active particles, *Part. Part. Syst. Charact.* 31 (2014) 317–336, <https://doi.org/10.1002/ppsc.201300231>.
- [22] X. Wang, L. Sun, R. Agung Susantyoko, Y. Fan, Q. Zhang, Ultrahigh volumetric capacity lithium ion battery anodes with CNT-Si film, *Nano Energy.* 8 (2014) 71–77, <https://doi.org/10.1016/j.nanoen.2014.05.020>.
- [23] M. Puff, CeraCharge™ – world’s first rechargeable solid-state SMD battery, in, *TDK Technol. Prod. Press Conf.* (2017) 1–3.
- [24] J. Liu, X. Chen, J. Kim, Q. Zheng, H. Ning, P. Sun, X. Huang, J. Liu, J. Niu, P.V. Braun, High volumetric capacity three-dimensionally sphere-caged secondary battery anodes, *Nano Lett.* 16 (2016) 4501–4507, <https://doi.org/10.1021/acs.nanolett.6b01711>.
- [25] Y. Gao, C. Cheng, J. An, H. Liu, D. Zhang, G. Chen, L. Shi, High tap density Li<sub>4</sub>Ti<sub>5</sub>O<sub>12</sub> anode materials synthesized for high rate performance lithium ion batteries, *Chemistryselect.* 3 (2018) 348–353, <https://doi.org/10.1002/slct.201702477>.
- [26] J. Ren, H. Ming, Z. Jia, Y. Zhang, J. Ming, Q. Zhou, J. Zheng, High tap density Li<sub>4</sub>Ti<sub>5</sub>O<sub>12</sub> microspheres: synthetic conditions and advanced electrochemical performance, *Energy Technol.* 5 (2017) 1680–1686, <https://doi.org/10.1002/ente.201700069>.
- [27] W. Liu, Q. Wang, C. Cao, X. Han, J. Zhang, X. Xie, B. Xia, Spray drying of spherical Li<sub>4</sub>Ti<sub>5</sub>O<sub>12</sub>/C powders using polyvinyl pyrrolidone as binder and carbon source, *J. Alloys Compd.* 621 (2015) 162–169, <https://doi.org/10.1016/j.jallcom.2014.09.121>.
- [28] Y.H. Yin, S.Y. Li, Z.J. Fan, X.L. Ding, S.T. Yang, Synthesis of novel anode Li<sub>4</sub>Ti<sub>5</sub>O<sub>12</sub>/C with PAN as carbon source and its electrochemical performance, *Mater. Chem. Phys.* 130 (2011) 186–190, <https://doi.org/10.1016/j.matchemphys.2011.06.062>.
- [29] M. Duduta, B. Ho, V.C. Wood, P. Limthongkul, V.E. Brunini, W.C. Carter, Y.M. Chiang, Semi-solid lithium rechargeable flow battery, *Adv. Energy Mater.* 1 (2011) 511–516, <https://doi.org/10.1002/aenm.201100152>.
- [30] Y. Wu, Z. Wen, J. Li, Hierarchical carbon-coated LiFePO<sub>4</sub> nano-plate microspheres with high electrochemical performance for li-ion, *Batteries* (2011) 1126–1129, <https://doi.org/10.1002/adma.201003713>.
- [31] E. Pohjalainen, T. Rauhala, M. Valkeapää, J. Kallioinen, T. Kallio, Effect of Li<sub>4</sub>Ti<sub>5</sub>O<sub>12</sub> particle size on the performance of lithium ion battery electrodes at high C-rates and low temperatures, *J. Phys. Chem. C* 119 (2015) 2277–2283, <https://doi.org/10.1021/jp509428c>.
- [32] J. Guo, H. Guo, A.L. Baker, M.T. Lanagan, E.R. Kupp, G.L. Messing, C.A. Randall, Cold sintering: a paradigm shift for processing and integration of ceramics, *Angew. Chemie – Int. Ed.* 55 (2016) 11457–11461, <https://doi.org/10.1002/anie.201605443>.
- [33] H. Guo, A. Baker, J. Guo, C.A. Randall, Protocol for ultralow-temperature ceramic sintering: an integration of nanotechnology and the cold sintering process, *ACS Nano* 10 (2016) 10606–10614, <https://doi.org/10.1021/acsnano.6b03800>.
- [34] S. Funahashi, J. Guo, H. Guo, K. Wang, A.L. Baker, K. Shiratsuyu, C.A. Randall, Demonstration of the cold sintering process study for the densification and grain growth of ZnO ceramics, *J. Am. Ceram. Soc.* 100 (2017) 546–553, <https://doi.org/10.1111/jace.14617>.
- [35] J. Guo, H. Guo, D.S.B. Heiday, S. Funahashi, C.A. Randall, Semiconducting properties of cold sintered V<sub>2</sub>O<sub>5</sub> ceramics and Co-sintered V<sub>2</sub>O<sub>5</sub>-PEDOT:PSS composites, *J. Eur. Ceram. Soc.* 37 (2017) 1529–1534, <https://doi.org/10.1016/j.jeurceramsoc.2016.11.021>.
- [36] H. Guo, A. Baker, J. Guo, C.A. Randall, Cold sintering process: a novel technique for low-temperature ceramic processing of ferroelectrics, *J. Am. Ceram. Soc.* 3507 (2016) 3489–3507, <https://doi.org/10.1111/jace.14554>.
- [37] H. Guo, T.J.M. Bayer, J. Guo, A. Baker, C.A. Randall, Cold sintering process for 8 mol%Y<sub>2</sub>O<sub>3</sub>-stabilized ZrO<sub>2</sub> ceramics, *J. Eur. Ceram. Soc.* 37 (2017) 2303–2308, <https://doi.org/10.1016/j.jeurceramsoc.2017.01.011>.
- [38] J. Guo, N. Pfeifferberger, A. Beese, A.M. Rhoades, L. Gao, A. Baker, K. Wang, anne bolvari, C.A. Randall, Cold sintering Na<sub>2</sub>Mo<sub>2</sub>O<sub>7</sub> ceramic with polyetherimide (PEI) polymer to realize high performance composites and integrated multilayer circuits, *ACS Appl. Nano Mater.* (2018), <https://doi.org/10.1021/acsnan.8b00609>.
- [39] X. Zhao, J. Guo, K. Wang, T. Herisson De Beauvoir, B. Li, C.A. Randall, Introducing a ZnO-PTFE (Polymer) nanocomposite varistor via the cold sintering process, *Adv. Eng. Mater.* 1700902 (2018) 1–8, <https://doi.org/10.1002/adem.201700902>.
- [40] J. Guo, B. Legum, B. Anasori, K. Wang, P. Lelyukh, Y. Gogotsi, C.A. Randall, Cold sintered ceramic nanocomposites of 2D MXene and zinc oxide, *Adv. Mater.*

- 1801846 (2018) 1801846, <https://doi.org/10.1002/adma.201801846>.
- [41] J. Guo, S.S. Berbano, H. Guo, A.L. Baker, M.T. Lanagan, C.A. Randall, Cold sintering process of composites: bridging the processing temperature gap of ceramic and polymer materials, *Adv. Funct. Mater.* (2016) 7115–7121, <https://doi.org/10.1002/adfm.201602489>.
- [42] J.-H. Seo, J. Guo, H. Guo, K. Verlinde, D.S.B. Heidary, R. Rajagopalan, C.A. Randall, Cold sintering of a Li-ion cathode: LiFePO<sub>4</sub> -composite with high volumetric capacity, *Ceram. Int.* (2017), <https://doi.org/10.1016/j.ceramint.2017.08.077>.
- [43] J.H. Seo, K. Verlinde, J. Guo, D.S.B. Heidary, R. Rajagopalan, T.E. Mallouk, C.A. Randall, Cold sintering approach to fabrication of high rate performance binderless LiFePO<sub>4</sub>cathode with high volumetric capacity, *Scr. Mater.* 146 (2018) 267–271, <https://doi.org/10.1016/j.scriptamat.2017.12.005>.
- [44] S.S. Berbano, J. Guo, H. Guo, M.T. Lanagan, C.A. Randall, Cold sintering process of Li<sub>1.5</sub>Al<sub>0.5</sub>Ge<sub>1.5</sub>(PO<sub>4</sub>)<sub>3</sub> solid electrolyte, *J. Am. Ceram. Soc.* (2017) 2123–2135, <https://doi.org/10.1111/jace.14727>.
- [45] H. Leng, J. Huang, J. Nie, J. Luo, Cold sintering and ionic conductivities of Na<sub>3</sub>.256Mg<sub>0.128</sub>Zr<sub>1.872</sub>Si<sub>2</sub>PO<sub>12</sub>solid electrolytes, *J. Power Sour.* 391 (2018) 170–179, <https://doi.org/10.1016/j.jpowsour.2018.04.067>.
- [46] Y. Liu, Q. Sun, D. Wang, K. Adair, J. Liang, X. Sun, Development of the cold sintering process and its application in solid-state lithium batteries, *J. Power Sour.* 393 (2018) 193–203, <https://doi.org/10.1016/j.jpowsour.2018.05.015>.
- [47] J. Guo, A.L. Baker, H. Guo, M. Lanagan, C.A. Randall, Cold sintering process: a new era for ceramic packaging and microwave device development, *J. Am. Ceram. Soc.* 100 (2017) 669–677, <https://doi.org/10.1111/jace.14603>.
- [48] L. Gao, S.W. Ko, H. Guo, E. Hennig, C.A. Randall, Demonstration of copper Co-Fired (Na, K)NbO<sub>3</sub> multilayer structures for piezoelectric applications, *J. Am. Ceram. Soc.* (2016) 1–7, <https://doi.org/10.1111/jace.14207>.
- [49] X. Wu, Y. Guo, J. Su, J. Xiong, Y. Zhang, L. Wan, Carbon-Nanotube-Decorated Nano-LiFePO<sub>4</sub> @ C Cathode Material with Superior High-Rate and Low-Temperature Performances for Lithium-Ion Batteries, 5 (2013) pp. 1155–1160. doi: 10.1002/aenm.201300159.
- [50] B. Wei, J. Zhang, J. Liang, D. Wu, The mechanism of phase transformation from carbon nanotube to diamond, *Carbon N. Y.* 36 (1998) 997–1001, [https://doi.org/10.1016/S0008-6223\(97\)00232-7](https://doi.org/10.1016/S0008-6223(97)00232-7).
- [51] R.S. Alencar, W. Cui, A.C. Torres-Dias, T.F.T. Cerqueira, S. Botti, M.A.L. Marques, O.P. Ferreira, C. Laurent, A. Weibel, D. Machon, D.J. Dunstan, A.G. Souza Filho, A. San-Miguel, Pressure-induced radial collapse in few-wall carbon nanotubes: a combined theoretical and experimental study, *Carbon N. Y.* 125 (2017) 429–436, <https://doi.org/10.1016/j.carbon.2017.09.044>.
- [52] M. Taravillo, E. Flahaut, M. About, T. Article, Raman spectra of double-wall carbon nanotubes under extreme uniaxial stress, *Nano* (2008) 1–3, <https://doi.org/10.1021/nl080760o>.
- [53] F. Zhang, J. Shen, J. Sun, Y.Q. Zhu, G. Wang, G. McCartney, Conversion of carbon nanotubes to diamond by spark plasma sintering, *Carbon N. Y.* 43 (2005) 1254–1258, <https://doi.org/10.1016/j.carbon.2004.12.019>.
- [54] A. Merlen, P. Toulemonde, S. Le Floch, G. Montagnac, T. Hammouda, O. Marty, A. San Miguel, High pressure-high temperature synthesis of diamond from single-wall pristine and iodine doped carbon nanotube bundles, *Carbon N. Y.* 47 (2009) 1643–1651, <https://doi.org/10.1016/j.carbon.2009.02.014>.
- [55] L.T. Sun, J.L. Gong, Z.Y. Zhu, D.Z. Zhu, S.X. He, Z.X. Wang, Y. Chen, G. Hu, Nanocrystalline diamond from carbon nanotubes, *Appl. Phys. Lett.* 84 (2004) 2901–2903, <https://doi.org/10.1063/1.1704856>.
- [56] M.G. Stevens, S. Subramoney, H.C. Foley, Spontaneous formation of carbon nanotubes and polyhedra from cesium and amorphous carbon, 1998, pp. 352–356.
- [57] J. Liu, K. Song, P.A. Van Aken, J. Maier, Y. Yu, Self-supported Li<sub>4</sub>Ti<sub>5</sub>O<sub>12</sub> - C nanotube arrays as high-rate and long- life anode materials for flexible li-ion batteries, *Nano Lett.* 14 (2014) 2597–2603, <https://doi.org/10.1021/nl5004174>.
- [58] K. Huo, X. Li, B. Gao, L. Wang, Q. Li, X. Peng, X. Zhang, J. Fu, P.K. Chu, Self-supporting and binder-free anode film composed of beaded stream-like Li<sub>4</sub>Ti<sub>5</sub>O<sub>12</sub>Nanoparticles for high-performance lithium-ion batteries, *ChemElectroChem* 3 (2016) 1301–1305, <https://doi.org/10.1002/celec.201600215>.
- [59] L. Sun, J. Wang, K. Jiang, S. Fan, Mesoporous Li<sub>4</sub>Ti<sub>5</sub>O<sub>12</sub> nanoclusters as high performance negative electrodes for lithium ion batteries, *J. Power Sour.* 248 (2014) 265–272, <https://doi.org/10.1016/j.jpowsour.2013.09.041>.
- [60] X. Sun, M. Hegde, Y. Zhang, M. He, L. Gu, Y. Wang, J. Shu, P.V. Radovanovic, B. Cui, Structure and electrochemical properties of spinel Li<sub>4</sub>Ti<sub>5</sub>O<sub>12</sub> nanocomposites as anode for lithium-ion battery, *Int. J. Electrochem. Sci.* 9 (2014) 1583–1596.
- [61] K.C. Hsiao, S.C. Liao, J.M. Chen, Microstructure effect on the electrochemical property of Li<sub>4</sub>Ti<sub>5</sub>O<sub>12</sub> as an anode material for lithium-ion batteries, *Electrochim. Acta* 53 (2008) 7242–7247, <https://doi.org/10.1016/j.electacta.2008.05.002>.
- [62] B. Kurc, A. Swiderska-Mocek, Properties of Li<sub>4</sub>Ti<sub>5</sub>O<sub>12</sub> as an anode material in non-flammable electrolytes, *J. Appl. Electrochem.* 44 (2014) 245–253, <https://doi.org/10.1007/s10800-013-0651-1>.
- [63] L. Sun, J. Wang, K. Jiang, S. Fan, Mesoporous Li<sub>4</sub>Ti<sub>5</sub>O<sub>12</sub>nanoclusters as high performance negative electrodes for lithium ion batteries, *J. Power Sour.* 248 (2014) 265–272, <https://doi.org/10.1016/j.jpowsour.2013.09.041>.